POLITECNICO
MILANO 1863

DIPARTIMENTO DI MECCANICA

mecc

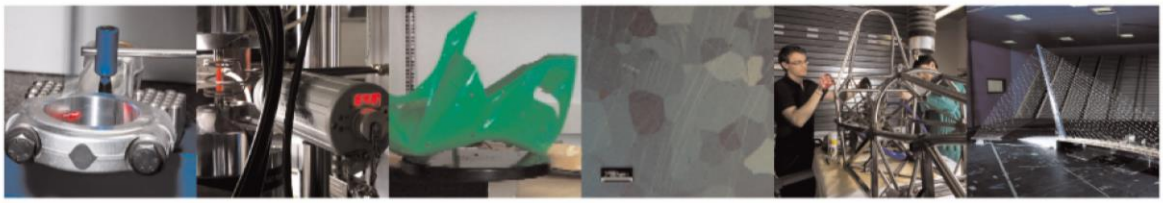

Molten pool temperature monitoring in laser metal deposition: Comparison between single wavelength and ratio pyrometry techniques

Maffia S., Furlan V., Previtali B.

This is a post-peer-review, pre-copyedit version of an article published in Maffia S., Furlan V., Previtali B., Molten pool temperature monitoring in laser metal deposition: Comparison between single wavelength and ratio pyrometry techniques, (2023) International Journal of Mechatronics and Manufacturing Systems, 16 (1), pp. 96 – 111. The final authenticated version is available online at: http://dx.doi.org/10.1504/IJMMS.2023.132027

This content is provided under CC BY-NC-ND 4.0 license

DIPARTIMENTO DI MECCANICA ■ POLITECNICO DI MILANO
via G. La Masa, 1 ■ 20156 Milano ■ EMAIL (PEC): pecmecc@cert.polimi.it
http://www.mecc.polimi.it
Rev. 0

Molten pool temperature monitoring in Laser Metal Deposition: comparison between single wavelength and ratio pyrometry techniques

Maffia Simone[a,*], Furlan Valentina[a], Previtali Barbara[a]

[a]*Department of Mechanical Engineering, Politecnico di Milano, Via La Masa 1, 20156 Milan, Italy*

*Corresponding author: simone.maffia@polimi.it

Molten pool temperature monitoring in Laser Metal Deposition: comparison between single wavelength and ratio pyrometry techniques.

Maffia Simone[a,*], Furlan Valentina[a], Previtali Barbara[a].

[a]Department of Mechanical Engineering, Politecnico di Milano, Via La Masa 1, 20156 Milan, Italy

*Corresponding author: simone.maffia@polimi.it

Abstract

Realizing complex components in laser metal deposition (LMD) without process control can lead to heat accumulation due to varying heat dissipation capacities of the geometric features. Monitoring the temperature of the molten pool is crucial, and infrared pyrometry is a commonly employed technique. This study explores temperature monitoring using a coaxial pyrometer operating in two modes: single wavelength and ratio modes. The single wavelength pyrometer measures the target temperature through optical emission but requires knowledge of target emissivity. In contrast, the ratio pyrometer is more adaptable in LMD as it does not depend on emissivity information, but it can be affected by background interferences. Single wavelength and ratio pyrometry monitoring of the molten pool was tested in two deposition conditions, using either a small or a large laser spot, highlighting the importance of collecting the single wavelength temperature.

Keywords: directed energy deposition; additive manufacturing; laser metal deposition; process monitoring; non-contact temperature measurement; pyrometer.

Abbreviations

3D	Three-dimensional
AM	Additive manufacturing
BT [°C]	Brightness temperature
E [W/m^3]	Spectral irradiance
LLS	Large laser spot
LMD	Laser metal deposition
LPBF	Laser powder bed fusion
P [W]	Laser power
PFR [g/min]	Powder feed rate
R [-]	Spectral irradiance ratio
RT [°C]	Ratio temperature
SLS	Small laser spot
SW	Singe wavelength
T [°C]	Real temperature
v [mm/s]	Scan speed
α_1 [K]	First brightness temperature calibration constant
α_2 [-]	Second brightness temperature calibration constant
β_1 [K]	First ratio temperature calibration constant
β_2 [-]	Second ratio temperature calibration constant
ε_λ [-]	Spectral emissivity
λ [µm]	Wavelength

1. Introduction

Laser metal deposition (LMD) belongs to the directed energy disposition category of additive manufacturing (AM) processes. In LMD the components are realized layer upon layer delivering filler metallic alloy through a nozzle into a molten pool generated by a high-power laser interacting with the substrate. Micrometric and spherical powder is a common filler material. The laser beam and the powder stream are coaxial and move together according to specific path to build the layers. LMD allows the realization of free-form structures without the use of support material, with high productivity and efficiency [1].

Stability and reliability in LMD, and more in general in any metal AM process, can only be achieved by a fine tuning of the process parameters: laser power, scan speed and powder feed rate as well as layer height and hatch distance among all. Once the process parameters are established in a preliminary experimentation at sample level, they should be applied to the real geometry of functional components using an appropriate scanning strategy. To guarantee stable and reliable realization of complex 3D components, process monitoring is useful to detect drifts of the process during the deposition, such as overgrowth and undergrowth [2,3].

Process monitoring consists in acquiring one or more signals during the build and analysing its evolution for the identification of the process conditions. The on-line recorded signals can be related to process signatures or to the formation of defects. There are multiple configurations of sensors that can be employed to monitor AM processes. A setup composed by two coaxially mounted photodiodes operating in the visible and infrared ranges, respectively, was successfully used in LPBF to automatically predict the density of the printed parts [4]. Thermal cameras are also quite common in monitoring the LPBF process, since are useful to record the thermal history of the region around the molten and the projection of spatter from the molten pool [5–7].

Indeed, one meaningful variable that can be monitored is the temperature of the molten pool [8,9]. When the temperature is too high, the provided energy is excessive, and instability phenomena may arise. On the other hand, a low temperature suggests that the provided energy is insufficient to guarantee a reliable build. The most commonly used sensors for this purpose in LMD are pyrometers: devices capable of non-contact measuring a target temperature by its optical emission [10]. Indeed, it was extensively demonstrated that pyrometers are capable of detecting various kinds of defects that may arise in the deposited parts and that are linked to the molten pool temperature [11]. Not only LMD, but also other metal AM processes make use of pyrometers for process monitoring. As an example, the signal coming from a pyrometer was successfully used to identify and locate porosities formed during a laser powder bed fusion (LPBF) process [12].

Pyrometers can be divided into two main categories: single wavelength (SW) and ratio pyrometers. The former computes the temperature by measuring the spectral irradiance of the target at one specific wavelength (or range of wavelengths). The temperature measured by a SW pyrometer is called brightness temperature (BT) and is computed as in Eq. 1:

$$BT = \frac{\alpha_1}{\ln\left(\frac{\varepsilon_\lambda(T)}{E_\lambda}\right) + \alpha_2} - 273.15\ [°C] \qquad \textit{Eq. 1}$$

where α_1 and α_2 are two constants calibrated with a black body source, ε_λ is the target spectral emissivity at the pyrometer wavelength λ, E_λ is the measured spectral irradiance and T is the real temperature of the target. ε_λ must be known to compute a reliable BT. However, ε_λ depends, among other, by the temperature itself and is not known a-priori, and it can only be estimated. Hence, SW pyrometers are usually not used in LMD for measuring the molten pool temperature, since its emissivity can only be guessed [13].

Ratio pyrometers instead measure the spectral irradiance at two different wavelengths (or ranges of wavelengths) λ_1 and λ_2 and compute their ratio R, as in Eq. 2:

$$R = \frac{E_{\lambda_1}}{E_{\lambda_2}} \; [-] \qquad \textit{Eq. 2}$$

The temperature measured by a ratio pyrometer is called ratio temperature (RT) and is computed as in Eq. 3:

$$RT = \frac{\beta_1}{\ln(R) + \beta_2} - 273.15 \; [°C] \qquad \textit{Eq. 3}$$

where β_1 and β_2 are two constants that can be found by calibrating the pyrometer on a black body source. If the target is assumed to behave like a grey body between the two considered wavelengths (i.e., its emissivity is the same at the two wavelengths), RT is independent by the emissivity and matches the real target temperature. It should be noted that, generally, molten metals in the near-infrared region satisfy the grey body assumption. Thus, the ratio pyrometry approach is ideal for LMD and is indeed the most used. Moreover, ratio pyrometers are not affected by any source of possible attenuations (gasses and dust) on the measured signals (provided that the attenuation is the same on the two signals) [14] and correctly compute the temperature for targets smaller than the measuring area (provided that the background is much colder than the target) [13].

On the other hand, coming to practice, various factors may negatively affect the temperature measurement carried out by ratio pyrometers. First, errors may be caused by a non-perfect grey body behaviour of the target or by a non-homogeneous transmittance of the means between the target and the pyrometer lens. Another known source of error may be the size-of-the-source effect. Namely, uncertainties may arise due to environmental factors like reflected ambient radiation, and absorption and emission of radiation by interfering hot gasses [15]. Considering how pyrometers are employed in the LMD process for monitoring or control of the deposition conditions, temperature read errors

may cause catastrophic outcomes of the build. Xiao at al. experienced anomalies in measuring the melt pool temperature in laser metal welding with a ratio pyrometer [16]. Thus, they switched to SW mode in some conditions. They attributed the misreading of the device to the defocusing and refraction effect of the plasma plume released by the melt pool and to the nanoparticles. Gutknecht et al. demonstrated that BT should also be considered alongside RT when monitoring the molten pool temperature in LPBF. The RT indeed could suffer of its abovementioned limits that do not affect BT [17]. To authors' knowledge, there is no published work addressing limits raised by SW or ratio pyrometry in LMD.

In this work, a series of LMD experiments were carried out sensing the temperature of the molten pool with a coaxial pyrometer in both SW and ratio mode. The study examined two process conditions to replicate the flexibility of the LMD process in manufacturing. In fact, either fine details and features at lower production rates, or coarse features at high deposition rates but poor quality can be built with the same machine by adjusting the laser spot size on the working plane. Throughout this work, these conditions are referred to small laser spot (SLS) and large laser spot (LLS), respectively. These two process conditions were tested to investigate the influence of the molten pool size, hence of the presence of the background in the pyrometer field of view during LMD. Indeed, in SLS conditions the pyrometer measurement area, which is fixed at its minimum for the used optical scheme, is larger than the produced molten pool, making it collect also the emission coming from a portion of the background. On the other hand, in LLS conditions the molten pool fills the entire area that is sensed by the pyrometer. Three experimental campaigns were carried out producing different geometries (single tracks, tubes, and cubes) and changing the process parameters for intentionally inducing variations in the molten pool temperature. The paper shows that ratio pyrometry may produce erroneous results when background noise is present. Thus, under some circumstances, the SW signal analysis become fundamental for the detection of process drifts in LMD.

2. Materials and experimental setup

The experiments were conducted with a gas atomized AISI 316L produced by Carpenter Additive (Philadelphia, US) with particle size range between 45 μm and 106 μm. The substrates used in the experiment were 5 mm thick AISI 301.

Figure 1 shows the LMD setup used in this work. Figure 2 shows the optical scheme of the coaxial implementation of the pyrometer, and Figure 3 shows its hardware implementation on the deposition head.

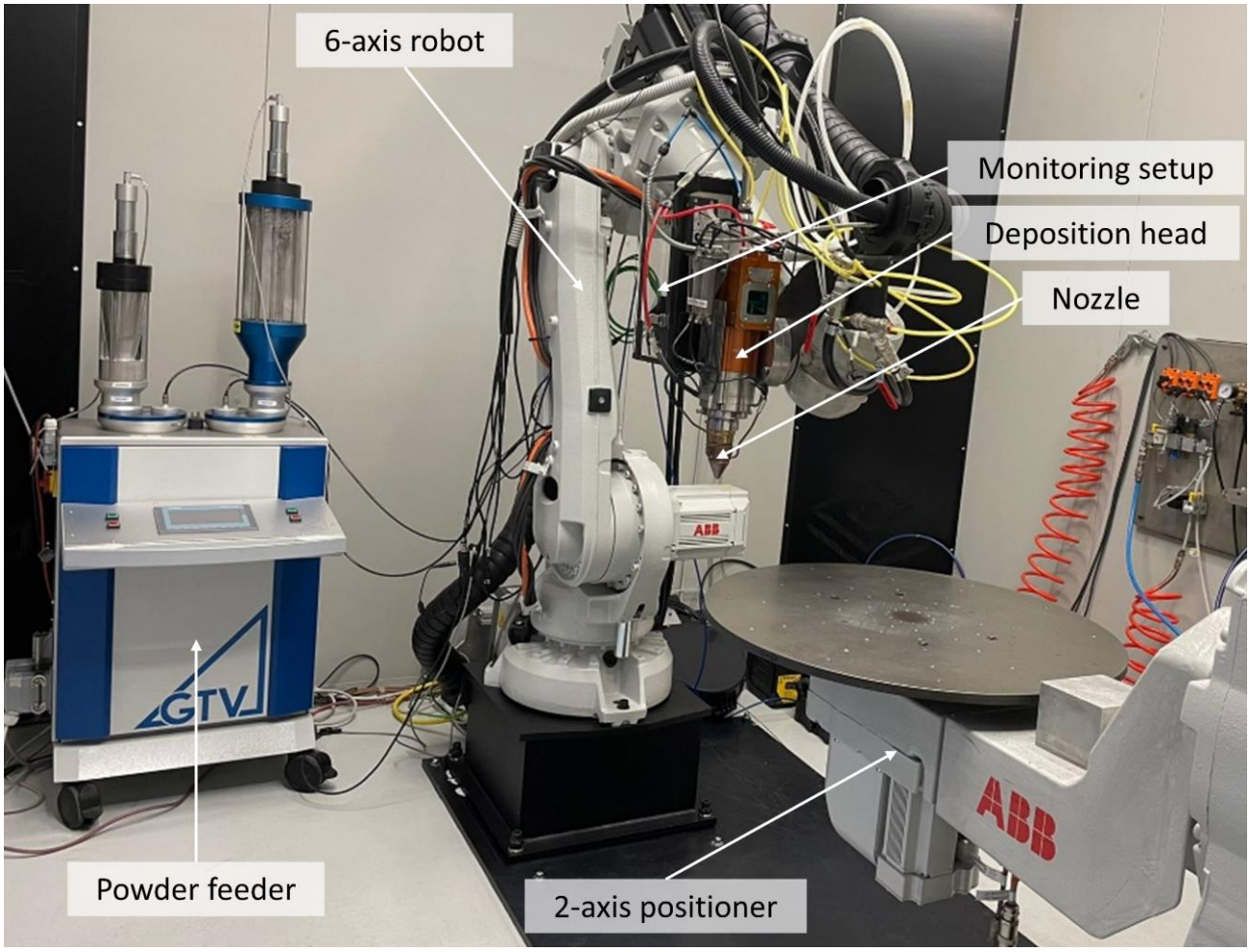

Figure 1 The LMD system used in this work.

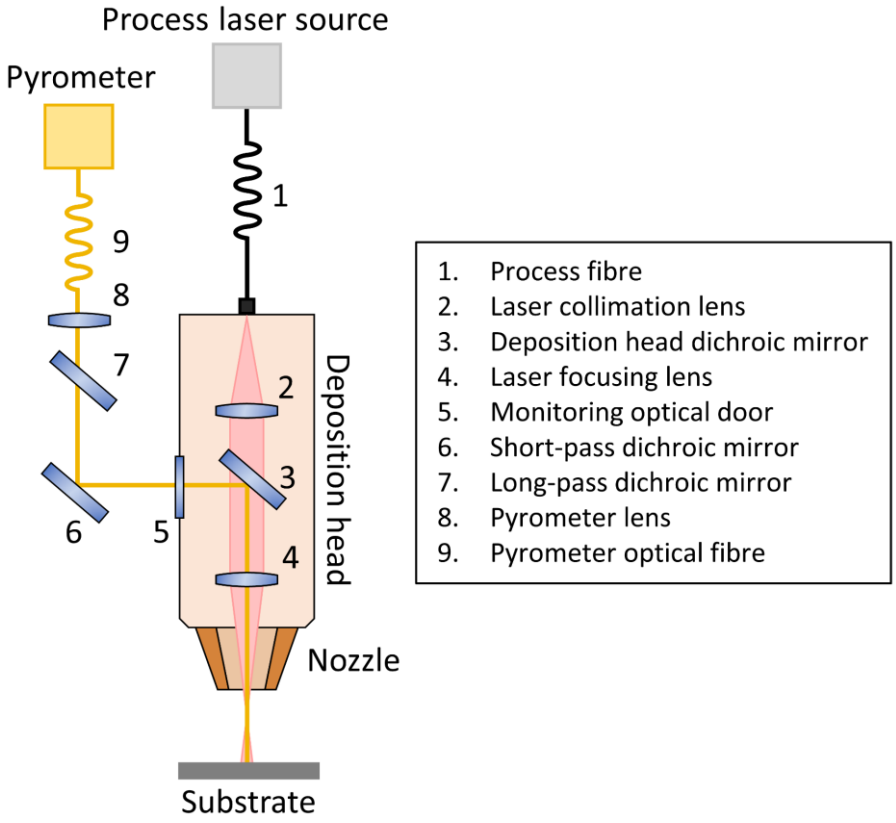

Figure 2 Optical scheme of the pyrometer setup coaxially integrated on the deposition head.

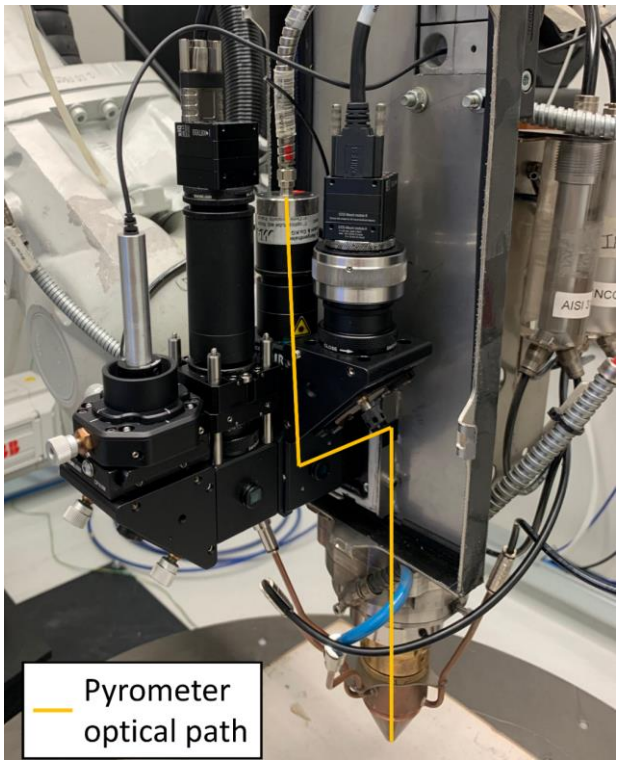

Figure 3 Hardware implementation of the monitoring system on the deposition head. The optical path of the pyrometer is also traced.

The experimental setup includes an IPG Photonics (Oxford, US) YLS-3000 active fibre laser source operating at 1070 nm and 3000 W of maximum power. A 400 μm process fibre delivers the laser beam to the Kuka AG (Augsburg, DE) MWO-I-Powder deposition head (element 1 in Figure 2). The focal lengths of the collimation and focusing lenses are 129 mm and 200 mm, respectively. The two lenses are the elements number 2 and 4 in the scheme of Figure 2. Adjusting the collimation, the laser spot diameter ranges between 0.7 mm and 3.5 mm on the working plane. A COAX-40-F coaxial nozzle from Fraunhofer ILT (Aachen, DE) was used. The powder feeding system is a GTV Verschleißschutz GmbH (Luckenbach, DE) TWIN PF 2/2-MF. Argon serves as carrier and process shielding gas. The LMD setup is completed by an ABB Ltd (Västerås, SE) system composed by a 6-axis anthropomorphic robot (IRB 4600-45) coupled with a 2-axis positioner (IRBP A-250) for the deposition head movement and for the substrate handling, respectively.

A Lascon LPC04 high-speed fibre coupled infrared two-colour pyrometer by Dr. Mergenthaler GmbH & Co. KG (Neu-Ulm, DE) provides sensing of the molten pool temperature. The pyrometer operates over the wavelength bands: 1.60 – 1.75 μm (first channel) and 1.70 – 2.00 μm (second channel). A 45° tilted dichroic mirror (element 3 in Figure 2), transparent to the fibre laser wavelength and reflective elsewhere, inside the deposition head, allows the coaxial integration of optical sensors for process monitoring purposes through a lateral optical door. The deposition head focusing lens collects and collimates the light emitted by the molten pool, which is then deflected by the dichroic mirror. The pyrometer optic (element 8 of Figure 2) with 45 mm of focusing length convey this light to the pyrometer body through an optical fibre (element 9 in Figure 2) with 400 μm of core diameter. With this optical configuration, the theoretical minimum diameter of the pyrometer field of view is 1.8 mm at its waist. On the working plane the diameter of the pyrometer field of view is 2.5 mm. Two other dichroic mirrors, one with 650 nm cut-off wavelength (element 6 in Figure 2) and one with 1180 nm cut-on wavelength (element 7 in Figure 2), lay between the deposition head and the

pyrometer optic for the implementation of other sensors, not addressed within this work. All the experimental campaigns described in this work were conducted using the pyrometer running in both SW and ratio modes. The BT was computed on the first range of wavelengths setting the emissivity of 0.27 [18].

2.1. Pyrometer calibration

The pyrometer was calibrated on a blackbody source calibrator HS-25-1000 from Dr. Mergenthaler GmbH & Co. KG (Neu-Ulm, DE). For the calibration, the pyrometer had to be mounted on the definitive optical chain to take into account all of the interposed optical elements between the pyrometer body and the working plane. Figure 4 shows a picture of the setup for the calibration procedure. The calibration was performed by stepwise imposing various known temperatures on the blackbody source, which has an emissivity of 0.995. The pyrometer acquires the spectral irradiances of the blackbody source on its two channels and computes the calibration constants (α_1 and α_2 and β_1 and β_2 of Eq. 1 and Eq. 3, respectively) by best-fitting the two signals with the known temperature. The imposed temperatures are 500°C, 600 °C, 700 °C, 800 °C, 900 °C and 990 °C.

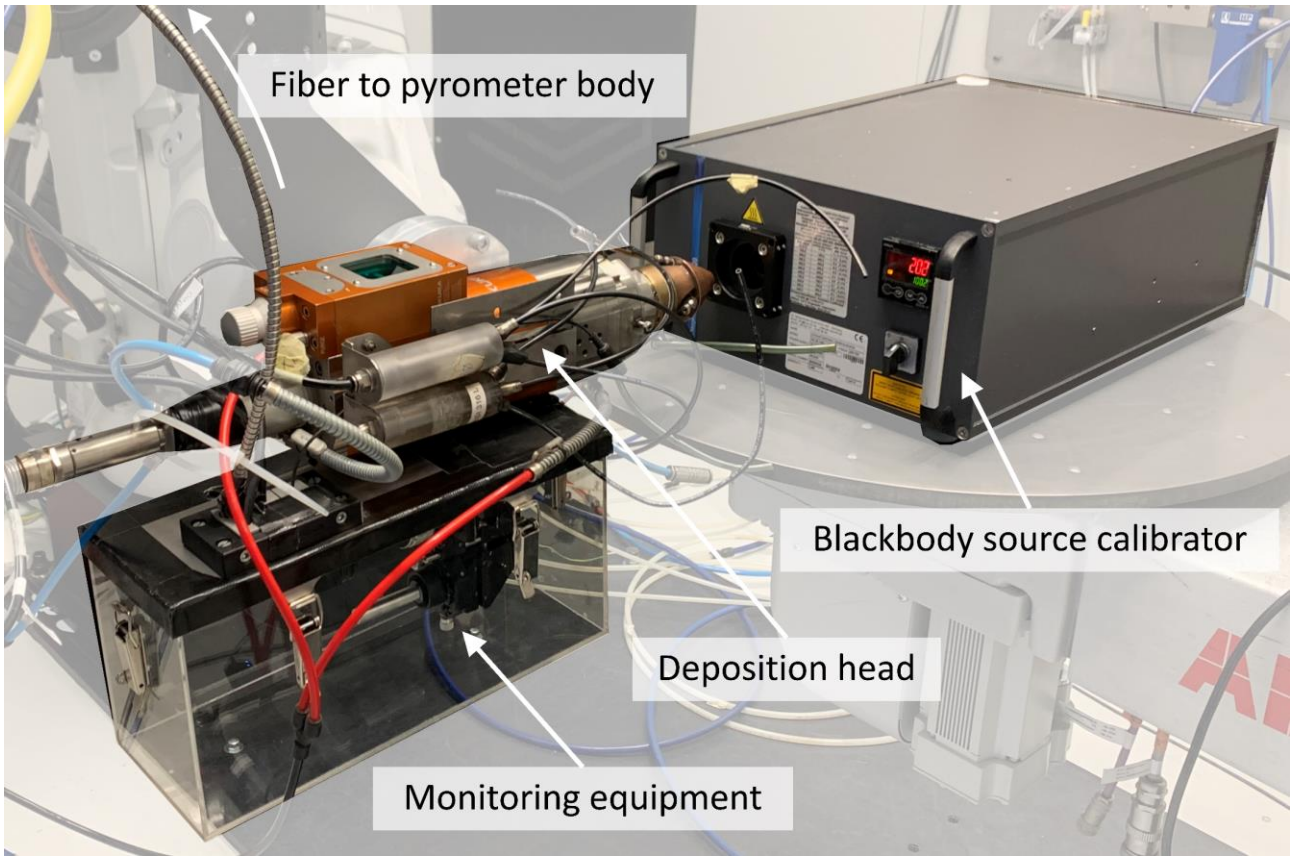

Figure 4 Setup for the calibration procedure.

3. Experimental campaigns

Three sets of experimental campaigns were carried out realizing single tracks, thin-walled tubes, and cubes. The samples were realized with both SLS and LLS tools. On the other hand, the pyrometer field of view on the working plane was fixed in all the experimentations. The purpose was to demonstrate the capabilities of the pyrometer in identifying the differences in the process status (namely: temperature variations) due to energetical and geometrical aspects using both the available pyrometer modes: SW and ratio modes. In the experimental campaign dealing with the deposition of single tracks, the variation of temperature was demanded only to the variation of energy input determined by process parameters. On the other hand, the variation of temperature in the tube depositions was due only to heat accumulation forced by geometrical aspects of the specimens.

Finally, when dealing with cubes, the temperature variation was due to both energetical and geometrical factors, combined. The specific experimental strategies for the chosen geometries are better explained in the next paragraphs.

In the experiments, the two running modes of the pyrometers are evaluated and compared in their ability of correctly spotting the induced variations of temperature in the tested conditions. Notice that, since the BT is not the real temperature due to the impracticality of knowing the exact emissivity of the material at any time, arbitrary units are used when reporting the BT. For this reason, BT was compared only qualitatively to RT, which is reported in °C since it does not require the knowledge of the current emissivity of the target. For the aim of this work, the only evaluation of the temperature trends in response to energy input or sample geometry was required.

3.1. Single tracks

Two separate experimental campaigns, one with SLS and one with LLS tool, were conducted: laser power (P), scan speed (v) and powder feed rate (PFR). A central composite design plan was chosen for these campaigns on single tracks to explore a wide range of process parameters (Table 1). The BT and the RT were measured during the depositions of the single tracks, and their median for each track were computed to investigate the effect of the process parameters on the measured temperatures in the two laser spot configurations. No replicates were realized for the axial and corner conditions of the experimental plan, and the central point was replicated six times to maintain the design rotatability. The runs are randomized. The obtained results are then summarized in main effect plots to obtain a visual representation of the temperature variations induced by the single process parameters. The purpose of this experiment is to investigate if the two working modes of the pyrometers produce comparable results in terms of temperature variations forced by the process parameters manipulation. An important aspect of single tracks is that the substrate (i.e., the background) does not heat up significantly during the deposition, staying cold.

Table 1 Process parameters for single tracks experimental campaigns.

Fixed parameter	SLS	LLS
Laser spot diameter, [mm]	1.2	2.5
Standoff distance, [mm]	10	7
Shielding gas flow rate, [L/min]	25	15
Carrier gas flow rate, [L/min]	7.5	4.5
Varied parameters		
Laser power, *P* [W]	285, 320, 370, 420, 455	600, 700, 850, 1000, 1100
Scan speed, *v* [mm/s]	8.5, 14.0, 22.0, 30.0, 35.5	8.6, 10.0, 12.0, 14.0, 15.4
Powder feed rate, *PFR* [g/min]	4, 6, 9, 12, 14	7, 9, 12, 15, 17

3.2. Tubes

Two thin-walled tubes with different diameters were realized with both SLS and LLS tools. The process parameters (Table 2) were fixed in the two configurations: only the diameter changes. The two levels of tube diameter are 14 mm and 24 mm. Hence, only the geometry can have an impact on the molten pool temperature: smaller diameter tubes are expected to accumulate more heat, inducing a rapid increment of the molten pool temperature. On the other hand, larger diameter tubes can dissipate heat faster, and a lower molten pool temperature is indeed expected. Indeed, using the same process parameters, and especially the same linear scan speed, the laser beam passes through the same angular position in a lower time interval when realizing the smaller tubes. In terms of numbers, the laser passes through the same angular coordinate in the smaller diameter tubes in approximately 60% of the time it takes to complete a full rotation in the larger diameter tubes. Also, since it is a long deposition, the background will get hot. A helical scanning strategy was used to realize the tubes by exploiting the vertical movement of the deposition head and the rotation of the 2-axis positioner. The nominal height of the tubes is 40 mm. One replicate per condition was realized, and the temperature signals are analysed in time domain.

Table 2 Process parameters for tubes experimental campaigns.

Fixed parameter	SLS	LLS
Laser spot diameter, [mm]	1.2	2.5
Laser power, *P* [W]	370	500
Scan speed, *v* [mm/s]	19	10
Powder feed rate, *PFR* [g/min]	9	9
Vertical increment, [mm]	0.25	0.50
Standoff distance, [mm]	10	7
Shielding gas flow rate, [L/min]	25	15
Carrier gas flow rate, [L/min]	7.5	4.5
Varied parameter		
Tube diameter, [mm]	14, 24	14, 24

3.3. Cubes

Three cubes were realized for each laser spot diameter condition, with three levels of laser power to induce temperature variations. The other process parameters were kept fixed (Table 3). When compared to scanning tubes of varying diameters, the temperature increment in this case is directly caused by the increase in energy density delivered to the powder by higher laser power [19]. Additionally, as tracks are overlapped and layers are deposited one after another, heat accumulates, causing the both the molten pool and the background to become increasingly hot. The base of the cubes is 10 mm x 10 mm, and the nominal height is 10 mm. The scanning strategy is bi-directional zig-zag. One replicate per condition was realized, and the temperature signals are analysed in time domain.

Table 3 Process parameters for cubes experimental campaigns.

Fixed parameter	SLS	LLS
Laser spot diameter, [mm]	1.2	2.5
Scan speed, *v* [mm/s]	19	10
Powder feed rate, *PFR* [g/min]	9	9
Vertical increment, [mm]	0.25	0.50
Hatch spacing, [mm]	0.35	0.70
Standoff distance, [mm]	10	7
Shielding gas flow rate, [L/min]	25	15
Varied parameter		
Laser power, *P* [W]	370, 470, 570	500, 600, 700

4. Results and discussions

Figure 5 reports BT and RT of the three experimental campaigns. RT data are shown in degrees Celsius, while BT ones are in arbitrary unit, as explained in chapter 3. Figure 6 shows the realized tubular and cubic samples.

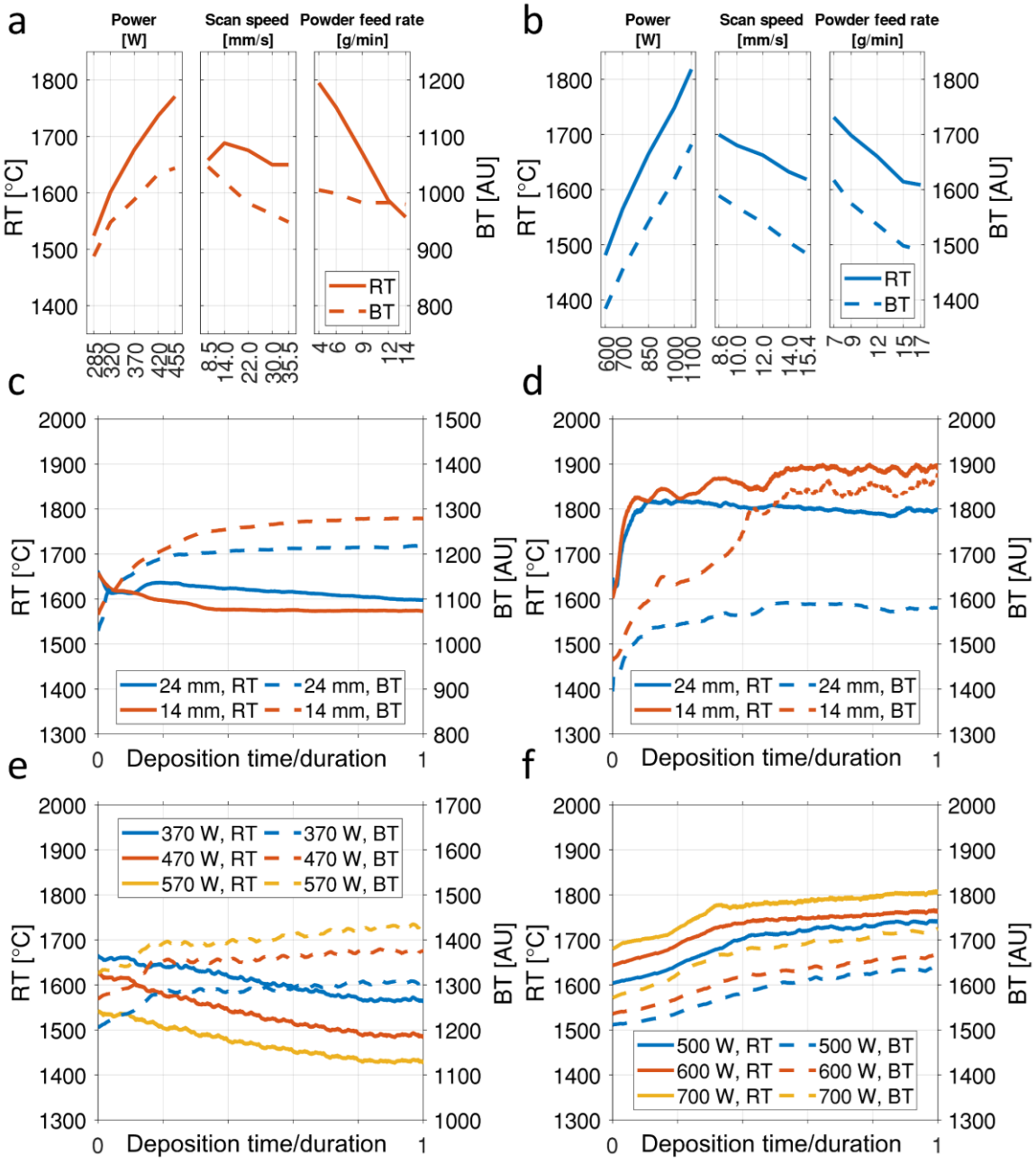

Figure 5 Results of the experimental campaigns: main effect plots of median temperatures of single tracks with (a) SLS and (b) LLS tools; BT and RT of tubes against normalized deposition time with (c) SLS and (d) LLS tools; BT and RT of cubes against normalized deposition time with (e) SSL and (f) LLS tools.

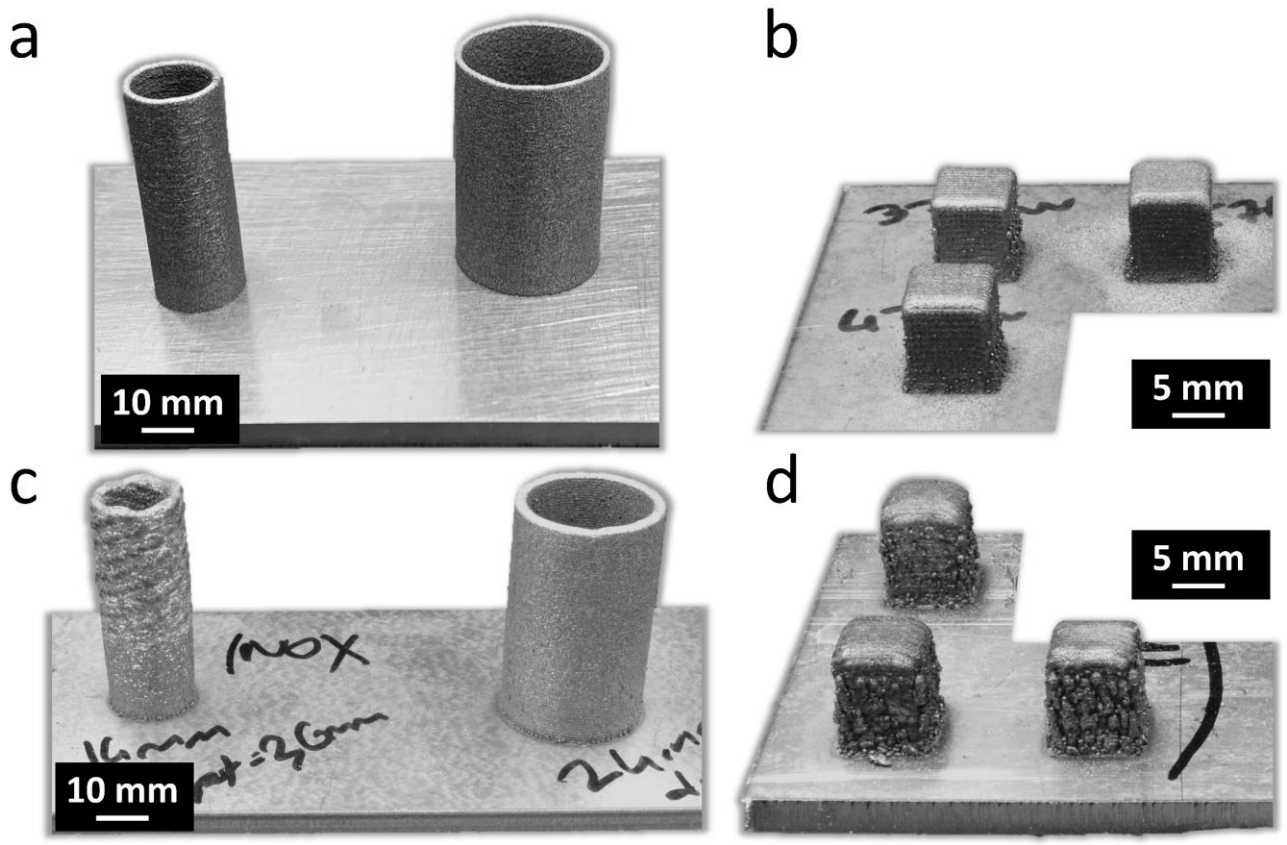

Figure 6 Realized samples: (a) tubes in SLS conditions, (b) cubes in SLS conditions, (c) tubes in LLS conditions, (d) cubes in LLS conditions.

The main effect plots of the single tracks median temperatures (Figure 5-a and Figure 5-b) show that in most generally an increment of the provided energy (by rising *P* or by reducing *v*) induces an increment of the molten pool temperature. On the other hand, the temperature decreases by increasing the *PFR*, since the mass to be melted is larger. BT and RT show the same reasonable trend in both SLS and LLS conditions, in accordance to literature [20]. Considering Figure 5-a, the influence of *v* and *PFR* does not cause an identical effect in BT and RT. This may be explained by a variation of the shape of the molten pool or of its heat gradient [17], but this behaviour should be further investigated with an analysis of the molten pool frames acquired with a coaxial camera.

Figure 5-c and Figure 5-d reports the collected temperatures in tubes manufactured respectively with the SLS and LLS tools, while Figure 5-e and Figure 5-f report the results of cubes realized respectively in the two different conditions (moving median filter is applied to data to enhance

readability). In tubes, the expected trend of the molten pool temperature is that it should be higher in the small diameter tubes due to poor heat dissipation. This is also clearly visible in the 14 mm tube of Figure 6-c, which shows clear signs of overheating. Considering cubes instead, according also to the results obtained with single tracks, the molten pool temperature is expected to be higher when a higher laser power is used. Indeed, the power directly determines the amount of energy that is provided to the material to be melted. In both the experiments, BT and RT are concurring when LLS tools are used (namely: temperature increases when tube diameter reduces due to higher heat accumulation, and also when the laser power rises in cubes), following the expectations. On the other hand, BT and RT are discordant in the SLS conditions: while BT behaves as in the LLS experiments, correctly spotting heat accumulations in both tubes and cubes, RT follows the opposite trend. Hence, considering only RT, it is possible to obtain misleading information about the process status. In the case that RT is used as the control variable in a LMD feedback control system in SLS conditions, the actions of the controller will enhance the process drifts instead of mitigating them, since heat accumulations make RT to reduce. Indeed, under this supervised process conditions, the real behaviour of the molten pool temperature is known and manipulated through process parameters and sample geometry, but this is not the case when a real component is considered, when process monitoring or control is actually necessary [21]. Two typical scenarios that are likely to verify when realizing a real complex component by LMD process are heat accumulation due to a thin feature being scanned multiple times in a short period of time or due to uncontrollable scan speed reduction when drastic variations of the scanning direction occur (in this last case, the energy increases in the point where the direction changes due to the unavoidable drop of scan speed). Using a pyrometer as monitoring device in LMD is meant exactly to identify these overheating scenarios when they cannot be easily predicted by simulation and, in case of its implementation as a process controlling device, to act against the problem by adjusting the laser power consequently. Unfortunately, this work

showed that, even though the advantage of using a ratio pyrometer instead of a SW one is clear, it is not always able to produce reliable results, under some circumstances.

This anomaly in SLS experiments can be explained by the mismatch between the pyrometer field of view and the laser spot areas [22]: when the pyrometer spot is larger than the molten pool, the computation of RT is affected by the background. Figure 7 shows a visual representation of: i) laser spot, ii) pyrometer field of view, iii) molten pool. The influence of the background is present only in SLS conditions. In the case of cold background (i.e., the single tracks experiments) RT is reliable, since little disturbances affect the measurements [16]. In the case of hot background (that happens during the deposition of tubes and cubes) the pyrometer also collects the irradiance around the molten pool, that disturbs the RT computation. The background radiation also affects the measurement of BT. However, since BT is concordant with the irradiance by Eq. 1, it correctly spots the process drifts. Hence, when the molten pool does not entirely fill the pyrometer field of view, BT should be considered instead of RT. A similar behaviour was observed in LPBF and laser welding [16,17] but never reported for LMD, to the authors' knowledge.

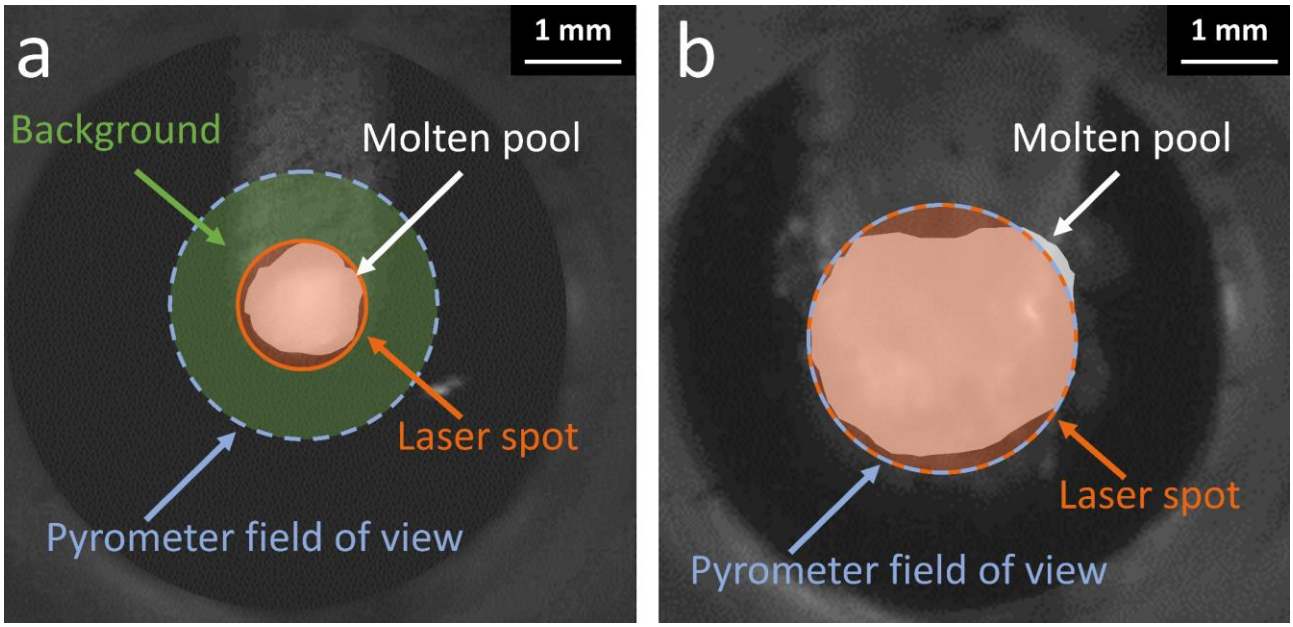

Figure 7 Scaled representation of the pyrometer field of view, the laser spot, the background, and the molten pool in (a) SLS and (b) LLS conditions (picture taken from a coaxial near infrared camera).

5. Conclusions

Three sets of experiments were carried out to study the molten pool sensing capabilities of a ratio pyrometer in LMD in both SW and ratio mode. The molten pool temperature was willingly manipulated by testing different sets of process parameters and geometrical characteristics of the produced samples.

- The BT is a good indicator of the process status, but since it directly depends on the emissivity of target (namely, the molten pool), the correct temperature cannot be measured, unless one has the emissivity behaviour as a function of material and temperature. On the other hand, the RT is not affected by the emissivity of the target if this shows a grey body behaviour. With metals, this condition is generally met, and the RT is close to the real temperature of the target.
- If the molten pool does not entirely fill the pyrometer field of view, disturbances related to the hot background may severely affect the computation of the RT when building multi-layer

structures, leading also to the total misinterpretation of the data. BT would also be affected, but it can clearly identify accumulated heat.

- BT should be considered rather than RT for measuring the molten pool temperature in LMD when a SLS tool is required for the realization of high-quality features unless the field of view of the pyrometer can be reduced to match the molten pool size. Instead, when a high deposition rate is required with a LLS tool, RT is a reliable indicator of the process status.

Similarly to what was already reported in previous studies for other applications, the importance of considering also the BT signal of a pyrometer, alongside the RT, was demonstrated for the LMD process with this work. Provided these findings, future developments of this work may be the development of an algorithm that controls both the BT and the RT at the same time to assess the reliability of the readings, avoiding potentially catastrophic outcomes especially when dealing with process control. For this instance, also the integration of data coming from other monitoring sensors can be considered.

Acknowledgments

Nuovo Pignone Tecnologie S.R.L. (Baker Hughes) is acknowledged for granting the industrial PhD scholarship under which this work was developed. BLM S.P.A. (BLM Group) is acknowledged for the provided support through the supply of the used machine and monitoring equipment.

References

[1] D. Svetlizky, M. Das, B. Zheng, A.L. Vyatskikh, S. Bose, A. Bandyopadhyay, J.M. Schoenung, E.J. Lavernia, N. Eliaz, Directed energy deposition (DED) additive manufacturing: Physical characteristics, defects, challenges and applications, Materials Today. 49 (2021) 271–295. https://doi.org/10.1016/j.mattod.2021.03.020.

[2] Z. Tang, W. Liu, Y. Wang, K.M. Saleheen, Z. Liu, S. Peng, Z. Zhang, H. Zhang, A review on in situ monitoring technology for directed energy deposition of metals, Int J Adv Manuf Technol. 108 (2020) 3437–3463. https://doi.org/10.1007/s00170-020-05569-3.

[3] S. Maffia, V. Furlan, B. Previtali, Coaxial and synchronous monitoring of molten pool height, area, and temperature in laser metal deposition, Optics & Laser Technology. 163 (2023) 109395. https://doi.org/10.1016/j.optlastec.2023.109395.

[4] S. Jayasinghe, P. Paoletti, C. Sutcliffe, J. Dardis, N. Jones, P.L. Green, Automatic quality assessments of laser powder bed fusion builds from photodiode sensor measurements, Prog Addit Manuf. 7 (2022) 143–160. https://doi.org/10.1007/s40964-021-00219-w.

[5] L. Yang, L. Lo, S. Ding, T. Özel, Monitoring and detection of meltpool and spatter regions in laser powder bed fusion of super alloy Inconel 625, Prog Addit Manuf. 5 (2020) 367–378. https://doi.org/10.1007/s40964-020-00140-8.

[6] M. Yakout, I. Phillips, M.A. Elbestawi, Q. Fang, In-situ monitoring and detection of spatter agglomeration and delamination during laser-based powder bed fusion of Invar 36, Optics & Laser Technology. 136 (2021) 106741. https://doi.org/10.1016/j.optlastec.2020.106741.

[7] T. Liu, C.S. Lough, H. Sehhat, Y.M. Ren, P.D. Christofides, E.C. Kinzel, M.C. Leu, In-situ infrared thermographic inspection for local powder layer thickness measurement in laser powder

bed fusion, Additive Manufacturing. 55 (2022) 102873. https://doi.org/10.1016/j.addma.2022.102873.

[8] L. Tang, R.G. Landers, Melt Pool Temperature Control for Laser Metal Deposition Processes—Part II: Layer-to-Layer Temperature Control, Journal of Manufacturing Science and Engineering. 132 (2010). https://doi.org/10.1115/1.4000883.

[9] L. Tang, R.G. Landers, Melt Pool Temperature Control for Laser Metal Deposition Processes—Part I: Online Temperature Control, Journal of Manufacturing Science and Engineering. 132 (2010). https://doi.org/10.1115/1.4000882.

[10] Z. Yan, W. Liu, Z. Tang, X. Liu, N. Zhang, M. Li, H. Zhang, Review on thermal analysis in laser-based additive manufacturing, Optics & Laser Technology. 106 (2018) 427–441. https://doi.org/10.1016/j.optlastec.2018.04.034.

[11] R. Bernhard, P. Neef, H. Wiche, C. Hoff, J. Hermsdorf, S. Kaierle, V. Wesling, Defect detection in additive manufacturing via a toolpath overlaid melt-pool-temperature tomography, Journal of Laser Applications. 32 (2020) 022055. https://doi.org/10.2351/7.0000055.

[12] J.A. Mitchell, T.A. Ivanoff, D. Dagel, J.D. Madison, B. Jared, Linking pyrometry to porosity in additively manufactured metals, Additive Manufacturing. 31 (2020) 100946. https://doi.org/10/ggvc6w.

[13] B. Müller, U. Renz, Development of a fast fiber-optic two-color pyrometer for the temperature measurement of surfaces with varying emissivities, Review of Scientific Instruments. 72 (2001) 3366–3374. https://doi.org/10/cxd2sx.

[14] D. Lowe, G. Machin, M. Sadli, Correction of temperature errors due to the unknown effect of window transmission on ratio pyrometers using an in situ calibration standard, Measurement. 68 (2015) 16–21. https://doi.org/10.1016/j.measurement.2015.02.043.

[15] D. Ketui, F. Chi, G. Shan, Single wavelength and ratio pyrometry reflection errors in temperature measurement of gas turbine blade, Measurement. 86 (2016) 133–140. https://doi.org/10.1016/j.measurement.2016.02.054.

[16] X. Xiao, X. Liu, M. Cheng, L. Song, Towards monitoring laser welding process via a coaxial pyrometer, Journal of Materials Processing Technology. 277 (2020) 116409. https://doi.org/10.1016/j.jmatprotec.2019.116409.

[17] K. Gutknecht, M. Cloots, K. Wegener, Relevance of single channel signals for two-colour pyrometer process monitoring of laser powder bed fusion, International Journal of Mechatronics and Manufacturing Systems. 14 (2021) 111–127. https://doi.org/10.1504/IJMMS.2021.119152.

[18] H. Fukuyama, H. Higashi, H. Yamano, Thermophysical Properties of Molten Stainless Steel Containing 5 mass % B4C, Nuclear Technology. 205 (2019) 1154–1163. https://doi.org/10.1080/00295450.2019.1578572.

[19] M. Lison, W. Devesse, D. de Baere, M. Hinderdael, P. Guillaume, Hyperspectral and thermal temperature estimation during laser cladding, Journal of Laser Applications. 31 (2019) 022313. https://doi.org/10.2351/1.5096129.

[20] S.J. Wolff, Z. Gan, S. Lin, J.L. Bennett, W. Yan, G. Hyatt, K.F. Ehmann, G.J. Wagner, W.K. Liu, J. Cao, Experimentally validated predictions of thermal history and microhardness in laser-deposited Inconel 718 on carbon steel, Additive Manufacturing. 27 (2019) 540–551. https://doi.org/10/ggcqv6.

[21] L. Song, V. Bagavath-Singh, B. Dutta, J. Mazumder, Control of melt pool temperature and deposition height during direct metal deposition process, Int J Adv Manuf Technol. 58 (2012) 247–256. https://doi.org/10.1007/s00170-011-3395-2.

[22] A. Núñez-Cascajero, A. Tapetado, S. Vargas, C. Vázquez, Optical Fiber Pyrometer Designs for Temperature Measurements Depending on Object Size, Sensors. 21 (2021) 646. https://doi.org/10.3390/s21020646.

List of tables

List of figures